Characterization of random fields and their impact on the mechanics of geosystems at multiple scales

Qiushi Chen[1], Andrew Seifried[2], José E. Andrade[1,*,†] and Jack W. Baker[2]

[1]*Engineering and Applied Science, California Institute of Technology, Pasadena, CA 91125, U.S.A.*
[2]*Department of Civil and Environmental Engineering, Stanford University, Stanford, CA 94305, U.S.A.*

SUMMARY

The behavior of particulate media, such as sands, is encoded at the granular-scale and hence methods for upscaling such behavior across relevant scales of interest—from granular-scale ($\sim 1\,\text{mm}$) to field-scale ($>1\,\text{m}$)—are needed to attain a more accurate prediction of soil behavior. Multi-scale analysis is especially important under extreme conditions, such as strain localization, penetration, or liquefaction, where the classical constitutive description may no longer apply. In this paper, internally consistent probabilistic models for undrained shear strength and Young's modulus are developed at multiple scales, and incorporated into a simulation framework where refinement of the material description to finer scales is pursued only as necessary. This probabilistic simulation approach is then coupled with the finite element method. Numerical examples are presented to show how the performance of the geosystem is influenced by taking into account multi-scale random fields. Copyright © 2010 John Wiley & Sons, Ltd.

1. INTRODUCTION

It is well known that material inhomogeneities exist at different length scales in geomechanical problems. Two types of inhomogeneities can be identified: (1) inherent inhomogeneities, which are those resulting from fluctuations in material properties, such as permeability or strength and (2) induced inhomogeneities, which are those imposed by a physical phenomenon (e.g. deformation) that alters the characteristics of the medium. Figure 1 shows typical scales relevant to granular materials. All the information pertaining to granular systems, including inhomogeneities, is encoded at the granular scale and propagated or upscaled through all the way to the field scale. It should be pointed out that the spatial randomness at the macroscale might be of a different stochastic nature than that of the grain scale, e.g. randomness in macroscopic Young's modulus versus randomness in particle elasticity. Although the scale of interest in this paper is still within the continuum domain, properties within this domain of interest may be fundamentally influenced by grain-scale properties.

Inherent inhomogeneities are commonly modeled through the use of random field theory and the finite element method (FEM). The effect of inhomogeneities on mechanical behavior of engineering problems has been studied by many researchers at a single scale. For instance, at the site scale,

---

*Correspondence to: José E. Andrade, Engineering and Applied Science, California Institute of Technology, Pasadena, CA 91125, U.S.A.
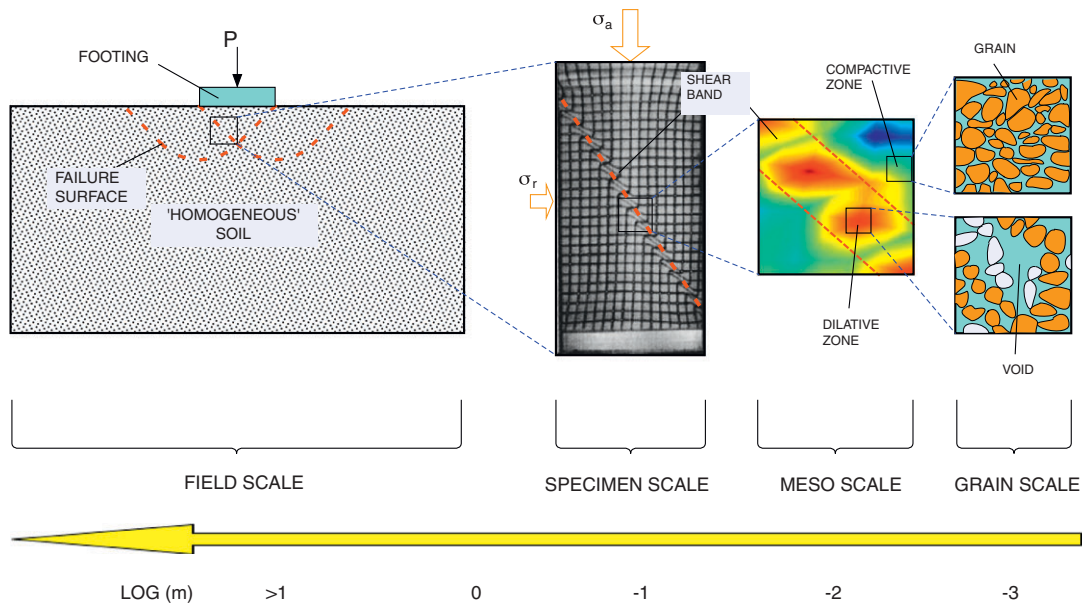†E-mail: j-andrade@northwestern.edu, jandrade@caltech.edu

Figure 1. Multi-scale nature of granular materials. After [1].

Griffiths and Fenton [2], Griffiths *et al.* [3], and Popescu *et al.* [4] have simulated shallow foundation resting on soils with spatially varying properties. It has been shown that inherent inhomogeneities of soil strength can greatly modify the basic form of failure mechanism of the foundation. More recently, Andrade *et al.* [1] have coupled advanced elastoplastic models with geostatistical tools to simulate the mechanical behavior of anisotropic samples of sands and showed that meso-scale inhomogeneities in the porosity trigger global instabilities that are responsible for a significant reduction in the load-carrying capacity of the samples. They have also observed that the upscaling of porosity fields delays the predicted onset of localization due to local averaging over mesh elements. In dealing with material inhomogeneities and their effects on geosystems across scales, the conventional methods need to be extended. Along this line, a multi-scale stochastic FEM has been recently developed [5–7]. In this approach, the original boundary value problem of random heterogeneous materials is decomposed into a slow (coarse)-scale deterministic BVP and a fast (fine)-scale stochastic BVP. The slow-scale problem is solved first using standard FEM and the solution is used as input for fast-scale BVP. In this paper, we propose methods to characterize random fields and to couple them with finite elements (FEs) at both coarse and fine scales.

Parallel to the development of modeling material inhomogeneities utilizing random field theory and the FEM, multi-scale methods have become the subject of intensive research during the past decade, especially for modeling heterogeneous materials. According to the taxonomy introduced in [8], multi-scale methods can be classified into four types, i.e. hierarchical, concurrent (strong coupling), semi-concurrent (weak coupling), and hybrid hierarchical-semiconcurrent. One of the motivations for these methods is to bypass the prohibitive computational cost of modeling macroscopic structures using more accurate micro-scale constitutive models. One such example is the FE^2 approach (e.g. [9, 10]) for modeling composite materials. In the FE^2 method, macroscopic constitutive equations at a material point are replaced by FE simulations of periodic microstructures. A strongly coupled multi-scale method was proposed [11–13] for analyzing nonlinear inelastic behavior for heterogeneous structures, where the macroscopic constitutive law is replaced by micro-scale FE computation at element level rather than at the material point. The above-mentioned methods deal with material behavior that is generally described by continuum constitutive laws at different scales. More recently, Andrade and Tu [14] and Tu *et al.* [15] proposed a framework coupling discrete element method with the FEM for behavior prediction in granular media,

where the phenomenological hardening laws at the macroscale are bypassed and the key material parameters are extracted from granular structures directly. While our paper focuses on material behavior described by continuum constitutive models, it is possible to extend it to couple with discrete models given the work done by Andrade and Tu [14] and Tu *et al.* [15].

In multi-scale models, the micro–macro relation is a key component. Various algorithms have been proposed in establishing micro–macro relations based on different assumptions dealing with either weakly coupled (e.g. [16, 17]) or strongly coupled (e.g. [11, 18]) scales. In the weakly coupled case, the micro- and macroscales can be fully separated and a representative volume element (RVE) or unit cell is typically used to represent the microstructure. In the strongly coupled case, the characteristic length of microscale is finitely smaller—rather than infinitely smaller—than that of macroscale. In this paper, we consider the case where different scales are strongly coupled and propose the use of a concurrent multi-scale scheme [8], where displacements from the macroscale are passed onto microscale as boundary conditions and the averaged stresses are passed back to macroscale. The assumptions here are that the strain and the stress, at an arbitrary material point in the macroscopic domain, are the volume average of the strain and stress fields over the microscopic domain, respectively.

A corresponding consideration in multi-scale modeling is the description of the underlying material properties at multiple scales. In this work, material properties (e.g. undrained shear strength and Young's modulus) are assumed to be random but varying spatially in a somewhat smooth manner. Mathematically, this means that these properties can be quantified as random variables at a particular location, and that the value of these variables at multiple locations can be described by joint probability distributions characterized using random fields modeling. Spatial dependence for the non-Gaussian fields is introduced by first transforming the variables of interest to have marginal Gaussian distributions, and then introducing dependence among these transformed variables through linear correlation coefficients—a procedure commonly used in the field of Geostatistics (e.g. [19]). Material properties at the coarse scale are defined by averaging values at the corresponding fine-scale locations; using this assumption, means, variances, and spatial correlations at the coarse scale are then derived to be internally consistent with the fine scale. A second important piece of multi-scale random fields is Monte Carlo simulation of realizations of the field at multiple scales. Thus, an iterative simulation procedure is adopted where simulated values are obtained at individual locations conditional on all previous simulations. This procedure is beneficial here because it allows one to first simulate the field at only the coarse scale, then add simulation points at the fine scale probabilistically consistent with the previous coarse-scale realizations. Furthermore, these conditional fine-scale simulations need not be performed immediately after the coarse-scale simulation, allowing one to start with a coarse-scale simulation, perform initial analysis on the system (either mechanics analysis or some other analysis of the soil properties), and then refine the scale of that simulation without having to start over or generate a new simulation of the field. This adaptive refinement is expected to have important practical advantages in some situations.

The paper is organized as follows. Section 2 provides a description of the random material properties of interest at the fine scale, including probability distributions and spatial dependence. The conditional simulation procedure described in the previous paragraph is also introduced. In Section 3, a multi-scale description of the random field is introduced, and the probability distributions and correlations at that scale are derived under the assumption that coarse-scale values are averages of corresponding fine-scale values. Strategies for multi-scale simulation are then discussed, including the feasibility of simulating entire fields at the coarse scale, and then refining that simulation by adding conditional simulations at the fine scale as desired. In Section 4, a multi-scale framework for coupling random fields and the FEM is proposed. Two main ingredients of the framework, e.g. element-splitting technique and concurrent information-passing scheme, are discussed in detail. In Section 5, numerical examples are presented where FE simulations of a strip footing utilizing the proposed framework are carried out. The undrained shear strength is treated as the random variable for bearing capacity analysis; the Young's modulus is treated as random for settlement analysis. Of particular interest is the impact of different degrees of fine-scale discretization on the overall performance of the geosystem.

2. CHARACTERIZATION OF MATERIAL PROPERTIES

The adopted approach for parameter simulation relies on classical random field models and Monte-Carlo methods modified to account for various scales of resolution throughout the sample. One of the challenges of this work is maintaining the appropriate spatial variability across scales. Characterization of both the distribution and spatial correlation of undrained shear strength, S_u, and Young's modulus, E, at the finest considered scale—the mesoscale—are detailed in this section.

2.1. Distribution of the soil properties

Beta, gamma, and lognormal distributions are all commonly used in the literature to model soil properties. While no sufficient data exists supporting one type over another, Popescu *et al.* [4] have observed that the values of soil strength in shallow layers are positively skewed. Based on these findings the lognormal distribution is used to describe each parameter, which can be represented by the following probability density function (PDF)

$$f_Y(y) = \frac{1}{y \sigma_{\ln Y} \sqrt{2\pi}} \exp\left(-\frac{1}{2}\left[\frac{\ln y - \mu_{\ln Y}}{\sigma_{\ln Y}}\right]^2\right) \tag{1}$$

where $f_Y(y)$ is used to denote the PDF and the values of $\mu_{\ln Y}$ and $\sigma_{\ln Y}$ are the mean and standard deviation of the natural log of the parameter Y, and are chosen depending on the parameter to be modeled. In this paper, the parameters (μ, σ) used for undrained shear strength and Young's modulus are (100, 50) kPa and (100, 50) MPa, respectively. Selection of these values is discussed in Section 5. Note that Y is used to denote the random variable and y is used to describe a specific numerical value of that variable.

The random variable can also be described in the form of a cumulative distribution function (CDF)

$$F_Y(y) = \Phi\left(\frac{\ln y - \mu_{\ln Y}}{\sigma_{\ln Y}}\right) \tag{2}$$

where $F_Y(y)$ denotes the CDF of Y and $\Phi()$ denotes the CDF for the standard normal distribution. A PDF from Equation (1) is plotted in Figure 2 alongside a histogram of simulated values. The histogram has the same general shape, but some variation is expected due to the finite number of realizations shown here.
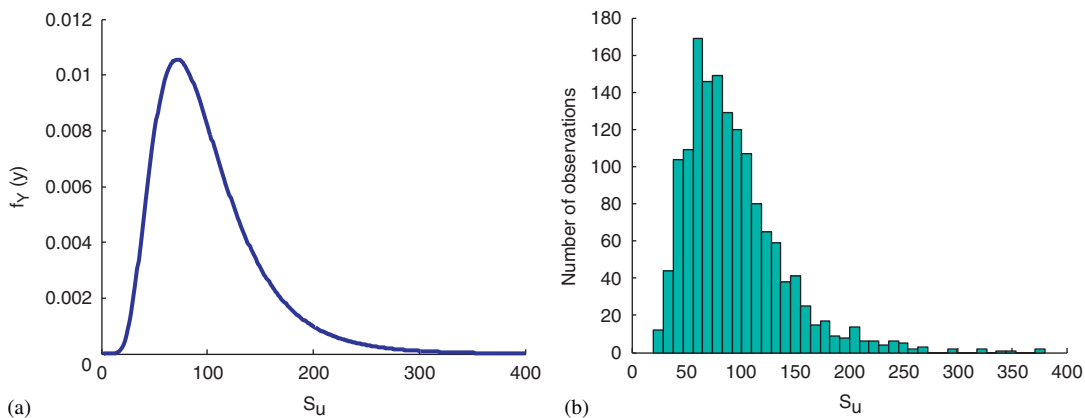

Figure 2. (a) Probability density function for undrained shear strength and (b) histogram of simulated values of undrained shear strength.

2.2. Normal score mapping

Realizations of the random variable at each point within the sample are dependent upon the values of the surrounding points (spatial relationships are considered in detail in the following section). For variables having Gaussian distributions, this joint dependence is fully described by pairwise linear correlation coefficients and the associated analytical equations are quite tractable. This is generally not true for non-Gaussian distributions where the associated model is not fully defined by a linear correlation coefficient, and thus a so-called normal-score mapping may be used to take advantage of the desirable Gaussian properties. In the next section, when working with fields of dependent variables, all the computations will be done using correlated Gaussian fields having a mean of zero and variance of unity. Each value in those standard Gaussian fields will then be transformed to have the target distribution of Equation (1) using the relationship

$$y = F_Y^{-1}(\Phi(z)) \tag{3}$$

where F^{-1} is the inverse CDF of the target distribution given in Equation (2), $\Phi()$ again denotes the CDF for the standard normal distribution, z represents a simulated value from the standard Gaussian distribution, and y is the transformed value coming from the target distribution. Figure 2(b) was created by simulating standard Gaussian samples (z) and transforming them using Equation (3), illustrating the validity of this transform. Note that in the particular application considered here, because Y is lognormally distributed, the transformation between Gaussian Z and lognormal Y can be performed by simply taking logarithms and exponentials, but this formulation is provided for generality.

It is assumed here that the spatial dependence introduced using this Gaussian correlation model and mapping technique is appropriate for describing the dependence of the variable being studied. Practical experience with this approach suggests that it is often a reasonable approximation [19], and because the distributions used here are not strongly non-Gaussian it is expected that dependence structure will not be significantly affected. When this transformation dramatically alters the distribution shape, the approximation may be less appropriate, although its practical advantages still make it a popular technique in those cases despite the approximation.

2.3. Spatial correlation

The probabilistic model of the previous section describes the distribution of a parameter value at a single location. To consider multiple locations in a specimen where the values at each location vary somewhat, spatial dependence must be taken into account. In this section, we will develop the mathematical tools for characterizing that dependence and simulating realizations of these random fields.

Spatial correlation is described here at the finest considered scale—the mesoscale—using a form of covariance known as a semivariogram, $\gamma(\mathbf{h})$, which is equal to half the variance of the difference between two random variables separated by distance $\mathbf{h}$

$$\gamma(\mathbf{h}) = \tfrac{1}{2} \text{Var}[Z(\mathbf{u}) - Z(\mathbf{u}+\mathbf{h})] \tag{4}$$

where $Z(\mathbf{u})$ is the distribution of the Gaussian random variable at location $\mathbf{u}$. The vector distance $\mathbf{h}$ accounts for both separation distance and orientation and may be defined by a scalar measure. To simplify the relationship between distance and semicovariance, we define a scalar distance measure

$$h = \sqrt{\left(\frac{h_1}{a}\right)^2 + \left(\frac{h_2}{b}\right)^2} \tag{5}$$

where h_1 and h_2 are the centroidal separation distances along the field's major and minor axes, respectively, corresponding to vector distance $\mathbf{h}$, and a and b specify how quickly spatial dependence decreases along those axes. When the 'a/b' ratio equals unity the sample is isotropic, meaning correlation decreases with distance equally in all directions. Skewing this ratio will result in banding of the sample.
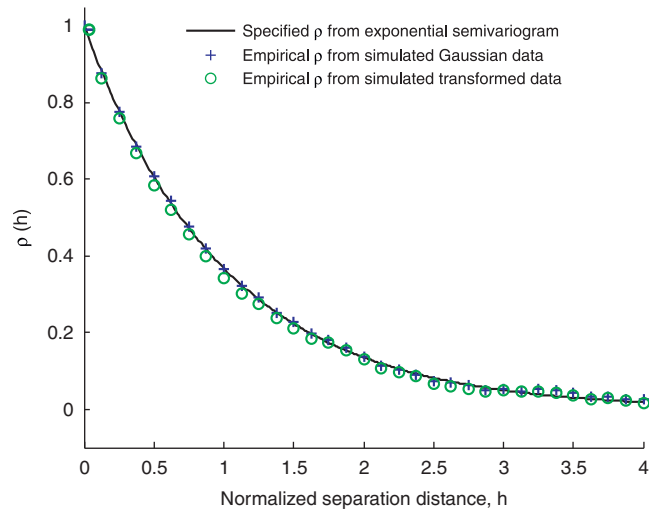
Figure 3. Empirical and specified correlations versus distance for a given realization of undrained shear strength.

The semivariogram is often used in geostatistics instead of covariance because it requires second-order stationarity of only the increments and not the underlying process. Here the two may be used interchangeably because both requirements are assumed to be satisfied, but semicovariance is used for the simulations because we are building on previous work that uses this formulation [19].

To generate samples consistent with a given semicovariance structure, we must specify a function that provides the semicovariance in Equation (4) for a given h. The samples above are generated according to the exponential semivariogram

$$\gamma(h) = 1 - \exp(-h) \tag{6}$$

Correlation, ρ, at a distance h is determined directly from the value of the semivariogram

$$\rho(h) = 1 - \gamma(h) \tag{7}$$

Note that the above equations describe spatial dependence of the Gaussian-distributed variables (Z) rather than the transformed variables having the final target distribution (Y). It is, therefore, necessary to verify that the desired spatial dependence relationship is upheld after the transformation of Equation (3) is performed. Figure 3 compares the specified model to the empirically calculated correlation of a simulated isotropic sample pre- and post-transformation (the procedure used to generate these data will be described in the following section). The slight difference between the specified correlation and the empirical correlation of the Gaussian data is due to the finite sample size. The difference between empirical correlation for the transformed data and the Gaussian data is due to the transformation. In this particular case the characteristics of the semivariogram are upheld well through the transformation from the Gaussian distribution to the lognormal distribution, but it is known that this correspondence will not always hold true for other marginal distributions [20].

2.4. Simulation

Given the specified correlation model from the previous section, we would now like to simulate sample data having that correlation structure. A sequential approach is taken here for the simulation procedure consisting of simulating each value individually, conditional upon all previously simulated values. While spectral-based simulation approaches are often preferable for random field simulation due to their stability and computational tractability, here a sequential correlation-based approach is utilized. It is believed that this approach will be particularly valuable if one desires to do adaptive refinement at fine scales; because it is not necessary to specify *a priori* the locations requiring fine-scale resolution, one can simply add additional fine-scale data, conditional upon all

previously simulated data, as the need arises. An additional advantage of this approach is that it allows real data points to be incorporated. No such measurements are included here, but may be used in future work to 'anchor' the simulated samples more closely to actual data. This would be accomplished by beginning the simulation with the field data included as previously generated variables, as outlined below, so that all simulated points are conditional upon them.

The first step in the sequential simulation process is to generate a single realization of a standard normal variable. All subsequent realizations are then conditional upon all previous realizations, represented by the joint distribution

$$\begin{bmatrix} Z_n \\ \mathbf{Z}_p \end{bmatrix} \sim N\left(\begin{bmatrix} 0 \\ \mathbf{0} \end{bmatrix}, \begin{bmatrix} \sigma_n^2 & \Sigma_{np} \\ \Sigma_{pn} & \Sigma_{pp} \end{bmatrix} \right) \tag{8}$$

where $\sim N(\boldsymbol{\mu}, \boldsymbol{\Sigma})$ denotes that the vector of random variables has a joint normal distribution with mean vector $\boldsymbol{\mu}$ and covariance matrix $\boldsymbol{\Sigma}$, Z_n is the next realization to be simulated, and $\mathbf{Z}_p$ is a vector of all previously defined or simulated points. The mean vector and covariance matrix have been partitioned to clarify several equations below. The subscripts n and p in the partitions represent 'next' (as in next point to be simulated) and 'previous' (as in all previously simulated points), respectively.

Individual terms inside the covariance matrix are defined by

$$\text{COV}[Z_i, Z_j] = \rho_{Z_i, Z_j} \cdot \sigma_{Z_i} \cdot \sigma_{Z_j} \tag{9}$$

where Z_i and Z_j refer to two locations within the random field at any scale with standard deviations σ_{Z_i} and σ_{Z_j}, respectively, and ρ_{Z_i, Z_j} is the correlation coefficient between them.

Given the above model, the conditional distribution of next realization to be simulated is given by a univariate normal distribution with updated mean and variance

$$(Z_n | \mathbf{Z}_p = \mathbf{z}) \sim N(\Sigma_{np} \cdot \Sigma_{pp}^{-1} \cdot \mathbf{z}, \sigma^2 - \Sigma_{np} \cdot \Sigma_{pp}^{-1} \cdot \Sigma_{pn}) \tag{10}$$

Once simulated, Z_n becomes a fixed data point in the vector $\mathbf{Z}_p$ to be conditioned upon by all subsequent realizations. This process is repeated until all the values in the field have been simulated.

3. MULTI-SCALE CONSIDERATIONS

One of the challenges of this work is maintaining appropriate spatial variability across several scales. This paper describes two scales of interest. The finer scale is denoted as scale 2, whereas the coarser scale is denoted as scale 1, and is defined as the average of all fine-scale points within its area. This relationship is visually represented in Figure 4 and is mathematically written as

$$Z_{1,a} = \frac{1}{n} \Sigma_{i=1}^n Z_{2,ai} \tag{11}$$

where the subscript a refers to the area in Figure 4 denoted as 'a'. All variables in the previous section were described at the fine scale. The effect of this relationship on moments of the random variables and their spatial relationships is described below.

Equation (11) implies that the (transformed) material properties at the coarse scale are the average values of the properties over corresponding areas at the fine scale. This relationship allows for explicit derivation of variances and spatial correlations of coarse-scale material properties, and the same averaging model will be used in the FE formulation. The optimal number of fine-scale elements to include in a coarse-scale element is likely to be problem dependent, as it balances benefits of computational efficiency with potential loss of fine-scale resolution. There are also considerations to be made with respect to the transformation between the target and normal distributions at the coarse scale, which is discussed in Section 3.2. Implications of the degree of resolution from a mechanics standpoint are explored in Section 5.3.
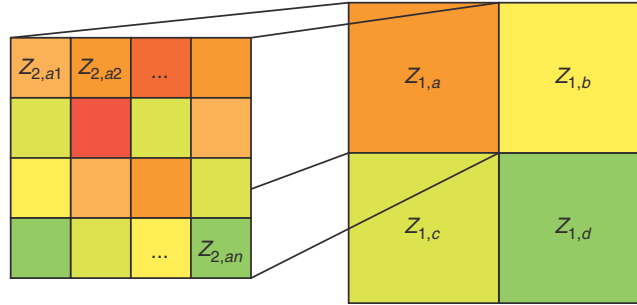
Figure 4. Graphical representation of material properties at 2 scales.

3.1. Moments and correlation for multiple scales

At the fine scale only, simulation of random fields is relatively straightforward. As discussed above, individual values in the field follow the standard Gaussian distribution with zero mean ($\mu_{Z_2} = 0$), unit standard deviation ($\sigma_{Z_2} = 1$), and correlation coefficients specified by Equation (7). These values are inserted into Equation (10) to perform sequential simulation of correlated fields.

Inclusion of a coarser scale requires more careful consideration. Means, standard deviations, and correlations are computed for coarse-scale z_1 values using the fine-scale information along with the definition of $Z_{1,a}$ (Equation (11)). Taking the expectation of this definition yields the mean of $Z_{1,a}$

$$\mu_1 = E[Z_{1,a}] = \frac{1}{n} \sum_{i=1}^{n} \mu_{2,i} = 0 \tag{12}$$

Accordingly, if the variance of fine-scale z_2 values is unity and the mean of coarse-scale z_1 values is zero as shown above, then the coarse-scale variance, $\sigma_{Z_{1,a}}$, can be computed as the expectation of Equation (11) squared (the variance is equal to the expectation of $Z_{1,a}^2$ in this case, since the mean of $Z_{1,a}$ is zero)

$$\sigma_{Z_1}^2 = E[Z_{1,a}^2] - 0 = \frac{1}{n^2} \sum_{i=1}^{n} \sum_{j=1}^{n} \rho_{z_{2i} z_{2j}} \cdot \sigma_{z_{2i}} \cdot \sigma_{z_{2j}} \tag{13}$$

Correlation must be defined between all considered scale combinations. Expanding the definition of covariance and rearranging Equation (9) to solve for correlation gives

$$\rho_{Z_i, Z_j} = \frac{\text{COV}[Z_i, Z_j]}{\sigma_{Z_i} \sigma_{Z_j}} \tag{14}$$

where Z_i and Z_j refer to two elements within the random field at any scale with means, μ_{Z_i} and μ_{Z_j}, and other terms as defined in Equation (9). Making the appropriate substitutions at each scale and simplifying yields the definition of correlation between two Z_1 elements (Equation (15a)) or between a Z_1 element and a Z_2 element (Equation (15b))

$$\rho_{Z1a, Z1b} = \frac{\sum_{i=1}^{n} \sum_{k=1}^{n} \rho_{Z2a_i, Z2b_k}}{\sum_{i=1}^{n} \sum_{j=1}^{n} \rho_{Z2a_i, Z2a_j}} \tag{15a}$$

$$\rho_{Z2, Z1a} = \frac{\sum_{i=1}^{n} \rho_{Z2, Z2a_i} \sigma_{Z2a_i}}{\sqrt{\sum_{i=1}^{n} \sum_{j=1}^{n} \rho_{Z2a_i, Z2a_j} \sigma_{Z2a_i} \sigma_{Z2a_j}}} \tag{15b}$$

where subscripts a and b refer to two different local averages as shown in Figure 4, and where scale 2 correlation was defined earlier in Equation (7). These results are comparable to corresponding results for Local Average Processes in Random Fields modeling [21], but differ slightly here in
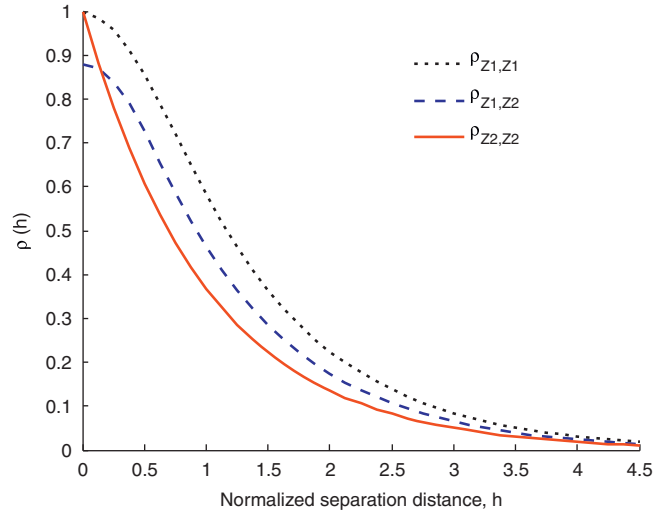
Figure 5. Correlation versus distance at all scales.

that they are defined for averages of discrete values rather than a continuous process. These results are used in later calculations and are needed to ensure consistency with the FEM.

Figure 5 compares correlation versus the normalized scalar distance measure between all combinations of scales. Note how averaging of the fine-scale points effectively increases correlation for a given distance relative to the fine scale. Nonlinear variation of correlation across the coarse scale puts more emphasis on fine-scale elements in closer proximity, which slightly increases correlation for a given centroidal distance. If correlation were to somehow vary linearly with distance, the correlations would be identical at all scales. This is similar to what occurs with fractal geometrical variations, although that type of correlation structure is not as easily incorporated into this spatial correlation characterization.

Also note how the correlation between a fine-scale element and a local average is not unity at a distance of zero, which is expected by the definition of inter-scale correlation given by Equation (15b). In this figure, each element at the coarse scale is subdivided into 16 fine-scale elements. If each element at the coarse scale comprised only a single fine-scale element, the correlation between scales at a distance of zero would be unity.

3.2. Normal-score mapping at the coarse scale

Figure 2 above verified that the target distribution is satisfactorily obtained through transformation at the fine scale, but it must be also verified that the mapping is consistent across scales. The challenge is that the variable Y_1 at the coarse scale is defined as the average of the fine-scale y_2 values within the coarse cell, but in the sections above, multi-scale averaging has been performed on the Gaussian variables Z. When mapping back the averaged (coarse-scale) z_1 values to coarse-scale y_1 values, we need to ensure that the distribution of Y is identical to what would be attained without this normal-score mapping.

There are several possibilities for performing this mapping at the coarse scale. In the first case, we do the transforming of the simulated z_2 values at the fine scale to get fine-scale y_2 values, and then average those fine-scale y_2 values to get a coarse-scale y_1 value

$$y_1 = \frac{1}{n} \sum_{i=1}^{n} F_{Y_2}^{-1}(\Phi(z_{2,i})) \tag{16}$$

This transformation would be guaranteed to ensure the averaging properties of Y, but it is not practically feasible as we will not simulate fine-scale y_2 values at all locations (this would eliminate the benefit of multi-scale simulation). It therefore becomes necessary to perform the transformation

directly on the coarse-scale y_1 values. Nonetheless, this method is used here as a benchmark for comparison of the other methods.

In a second case, we perform the transformation directly on the coarse-scale z_1 simulations, using the CDF of Y_1

$$y_1 = F_{Y_1}^{-1}\left(\Phi\left(\frac{z_1}{\sigma_{Z_1}}\right)\right) \tag{17}$$

In this mapping, we first re-normalize z_1 by dividing by its variance (it has mean zero, and the average of Gaussian variables is Gaussian, so no other normalization is necessary). We then transform it using the standard Gaussian CDF and the CDF of Y_1. Note that the CDF of Y_1 is not the same as the CDF of the fine-scale Y_2. This transformation is also guaranteed to ensure the averaging properties of Y, as we have explicitly used the desired marginal distribution of Y_1 in the transformation, but it requires the additional step of finding the marginal CDF of Y_1. In most cases this cannot be done analytically, but it is possible to estimate it through a relatively simple simulation procedure.

When estimating Y_1 for Equation (17), several alternatives are considered which vary in goodness of fit depending on the defined distribution of Y_2 and the number of fine-scale y_2 elements in each coarse-scale y_1 element. Realizations of Y_2 are first simulated and averaged. From here it is possible to compute the empirical CDF of Y_1 (this will be called Equation (17) alternate 1), which should generally be a good approximation if sufficient realizations are generated, but in order to have the convenience of a functional form two more methods are examined. As more fine-scale y_2 elements are included in each y_1 element, it becomes more appropriate to approximate Y_1 as Gaussian with estimated parameters (Equation (17) alternate 2). With fewer fine-scale y_2 elements included in each y_1 element—and when the distribution of Y_2 is similar to Gaussian—it may instead be appropriate to approximate Y_1 by the same form as that of Y_2, first taking care to update the parameters to reflect the effect of Equation (11) (Equation (17) alternate 3).

As a third transformation case, we simply use the fine-scale transformation but input coarse-scale z_1 values

$$y_1 \cong F_{Y_2}^{-1}(\Phi(z_1)) \tag{18}$$

The z_1 values have less than unit standard deviation (Equation (13)), so putting them through this transformation will result in coarse-scale y_1 simulations where value in the tails of the distribution is less likely. This is as desired due to the averaging process. There is no guarantee, however, that the y_1 values will have the desired marginal distribution in this case. Note that due to the central limit theorem, the marginal distribution of Y_1 will tend towards Gaussian as more fine-scale elements are included in the average. In particular, the quality of the approximate transformation of Equation (18) depends upon the similarity of the fine-scale distribution to a Gaussian distribution. This tendency may need to be accounted for by explicitly using the revised coarse-scale distribution in the mapping (Equation (17)). This is the simplest mapping of the above three cases, but the lack of guaranteed match with the desired marginal distribution is a disadvantage.

Figure 6 depicts empirical CDFs of coarse-scale elements obtained by three different methods. As mentioned above, the transformation of Equation (16) is considered the benchmark, but it is not feasible in this multi-scale context for obtaining coarse-scale values in the target distribution. It is obvious from the figure that in this case it is most appropriate to approximate the marginal distribution of Y_1 as lognormal (mapping by Equation (17) alternate 3 using the same form as Y_2 with the mean and standard deviation updated by Equations (12) and (13)). It is worth noting that this method works well for this particular fine-scale distribution and number of elements included in the coarse scale, but it is not guaranteed to work in a general sense, so a similar check is recommended for each particular distribution of Y_2 and degree of refinement.

An illustration of the case where it is not adequate to use the form of Y_2 for Y_1 is represented in Figure 7. Here, the y_2 values (for a hypothetical distribution of porosity) follow a truncated exponential model. As soon as these fine-scale y_2 elements are averaged to form a coarse-scale y_1 element, the extreme values of the distribution become much less likely. Thus, it is clearly
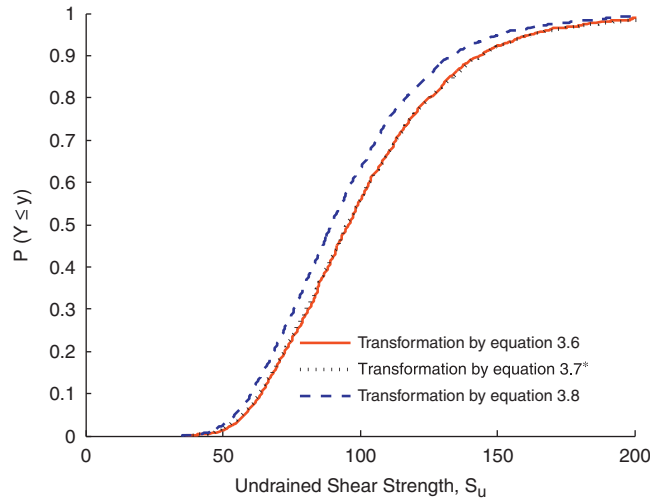
Figure 6. Empirical CDFs of simulations produced using several transformation approaches at the coarse scale (scale 1). The fine-scale (scale 2) properties are modeled as lognormal.
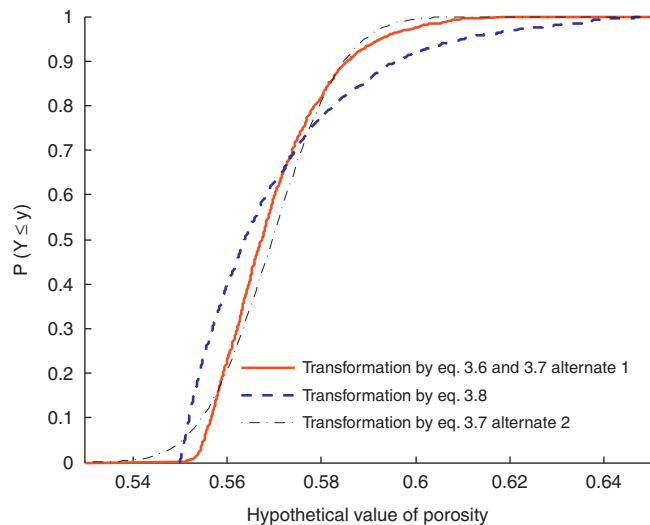

Figure 7. Empirical CDFs of simulations produced using several transformation approaches at the coarse scale (scale 1). The fine-scale (scale 2) properties are modeled as truncated exponential.

inappropriate to approximate the functional form of the coarse scale as that of the fine scale (either by Equation (18) or Equation (17) alternate 3). Instead, Figure 7 suggests that the best approximation of the true marginal CDF of Y_1 is the empirical CDF obtained as described above. Transformations performed directly on coarse-scale y_1 elements would be achieved by interpolating between the points derived for the empirical model. Note that the curves for Equations (16) and (17) alternate 1 are identical here because the same empirical model is used to visually represent each transformation. The purpose of including an additional example is to emphasize that in general it is advisable to evaluate all or most of these transformation options for the coarse scale: what works well in one situation may not work at all for another.

3.3. Implementation

The methodology here is based on defining parameters at the finest scale of consideration. The simulation will initially generate a coarse-scale resolution of the sample, then an empirically determined set of these are further refined to the fine scale. For refinement, the same conditional

framework described above is used with care taken to specify appropriate values of variance and correlation. The fact that the simulation begins at the coarse scale and works toward higher resolution should not result in a field any different than starting with a fine-scale field and subsequently averaging those elements together.

In the context of multiple scales, the sequential simulation process described above has the benefit of adaptive refinement (as introduced in Section 2). If deemed necessary at any point in time, any element can be broken down into its fine-scale components without consideration of sequence. A powerful implication of this is that the number of scales need not be limited to 2; while the above definitions explicitly consider two scales, they are easily expanded to more. The finest scale is always the scale at which the soil property's CDF and spatial correlation are defined, and any number of averaging scales can be defined relative to the fine scale using recursive applications of the equations above for coarse-scale properties. If it is desired to specify soil properties at the coarse scale, then the above multi-scale definitions and results of Figure 5 can be used to approximately invert for the fine-scale properties that result in the desired coarse-scale properties. With this approach, it may not even be necessary to specify in advance the number of scales to consider.

Even in the two-scale case presented here, computational expense can prove significant. As the size of $\mathbf{Z_p}$ increases, the computational demand of Equation (10) grows geometrically due to the need to invert ever-larger matrices. It therefore becomes desirable to limit the size of $\mathbf{Z_p}$ each time Equation (10) is evaluated. To achieve this, one option is to determine a maximum distance along each axis for which to consider previously generated realizations. Another is to limit the total number of previously simulated realizations to consider correlations with (keeping only those with the highest correlations). The latter approach is adopted for this research. The motivation for these approaches is that distant soil values have little impact on the distribution of Z_n, and that even nondistant points are 'shielded' from having an effect if there are many closer values with stronger correlations. These and other approaches are documented for single-scale conditional simulations [19], and appear to be generally applicable to multi-scale simulations as well.

Figure 8 shows that limiting the maximum number of previously generated elements with which to correlate to 125 does not adversely affect the specified spatial relationship significantly where correlation is significant. Correlation is indirectly upheld at distances greater than a radius inside which the maximum number of elements will fit. Some variations from the specified correlation are expected due to the finite sample size, but the discrepancy (relative to that in Figure 3) is more obvious when the maximum number of elements included in the operations precludes direct correlation. The threshold at which the additional discrepancy arises depends on the maximum number of points allowed in $\mathbf{Z_p}$ (with the discrepancy going to zero as an infinite number of points are allowed), so that this number can be varied to optimize the tradeoff between gained efficiency and lost accuracy.

As the simulation begins to refine coarse-scale elements, numerical instabilities must also be considered. As defined, the average value of all fine-scale z_2 values within a z_1 element must equal the originally simulated z_1 value. As a coarse-scale element is subdivided, the conditional variance given by Equation (10) will tend to decrease. For the last realization of Z_2 to be simulated, only one value exists such that the average is preserved, so that the conditional variance for that element will theoretically be zero. In practice, however, it is likely that the exact value will be slightly nonzero due to numerical approximations, so the simulation framework used for this research automatically sets this value appropriately. Failure to set this value manually may result in a negative (though extremely small) variance, which in turn results in an imaginary standard deviation after the inversion of Equation (10), and therefore unrealistic realizations of Z_2.

4. FRAMEWORK FOR COUPLING RANDOM FIELDS AND THE FEM AT MULTIPLE SCALES

In this section, a multi-scale framework that couples random fields and the FEM is presented. The formulation of the framework is based on the assumption that the strain and the stress
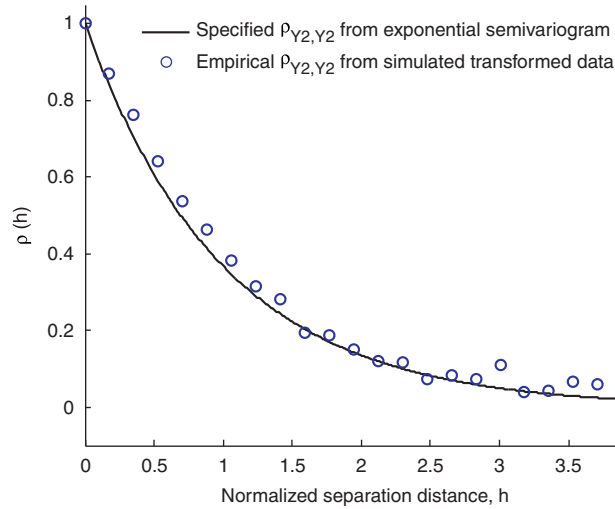
Figure 8. Empirical and specified correlations versus distance for a given realization of undrained shear strength, with the maximum number of conditioning elements to be considered limited to 125.

at an arbitrary material point in the coarse-scale domain are the volume average of the strain and stress fields over the fine-scale domain. In this paper, we focus on problems with material behavior being described by continuum constitutive theories. We utilize FEs at both the macro- and microscales. The kinematical constraints on the fine-scale domain are first discussed. Then, the main ingredients used to construct the framework, i.e. the element-splitting technique and the concurrent information-passing scheme are proposed.

4.1. Kinematical constraints on the fine-scale FEs

Derivation of the kinematical constraints on fine-scale elements is based on the assumption that strain at an arbitrary point at the coarse scale is the volume average of the strain fields over the fine-scale domain. Here, we follow the discussion from [22]

$$\varepsilon_1 = \frac{1}{\text{meas}(\Omega)} \int_\Omega \varepsilon_2(x) \, d\Omega \tag{19a}$$

$$\varepsilon_2 = \nabla^s u_2 \tag{19b}$$

where ε is the strain tensor, u is the displacement vector, subscripts '1' and '2' refer to macro- (coarse) and micro (fine)scales, respectively, 'meas(Ω)' is the measure of Ω, which equals to the volume (in 3D) or the area (in 2D) of the fine-scale domain, and ∇^s is the symmetric gradient operator. Only displacement fields that satisfy Equation (19) are said to be kinematically admissible. Furthermore, the fine-scale displacement field, u_2, can be split into the sum of a linear displacement, $\varepsilon_1 x_2$, where x is a position vector, and a displacement fluctuation, $\tilde{u}_2$, i.e.

$$u_2 = \varepsilon_1 x_2 + \tilde{u}_2 \tag{20}$$

The corresponding fine-scale strain field is then written as

$$\varepsilon_2 = \varepsilon_1 + \nabla^s \tilde{u}_2 \tag{21}$$

Substituting Equation (21) into Equation (19a), we have the kinematical constraint on displacement fluctuation as

$$\frac{1}{\text{meas}(\Omega)} \int_\Omega \nabla^s \tilde{u}_2 \, d\Omega = 0 \tag{22}$$
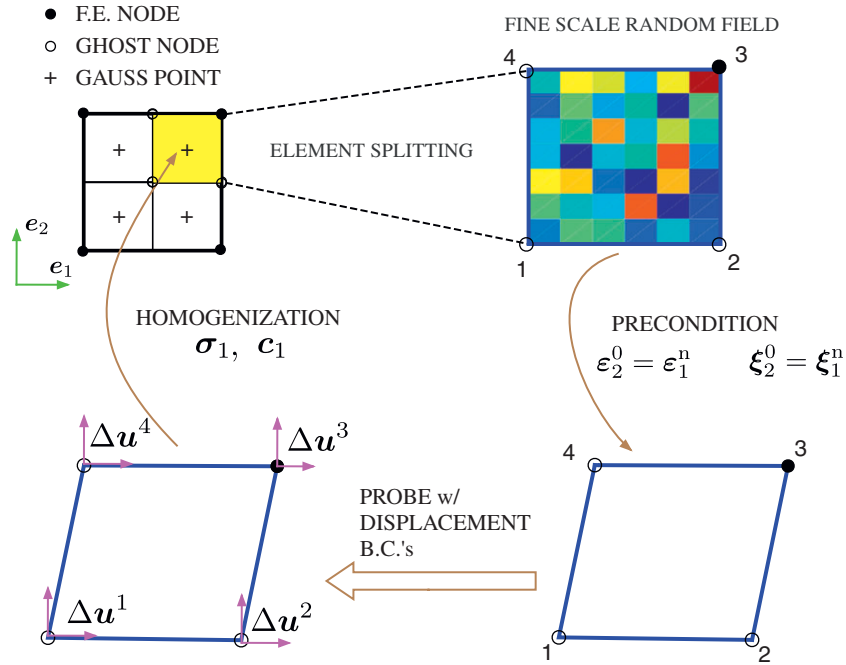
Figure 9. The multi-scale framework for coupling the FEM and random fields.

Depending on the choice of displacement fluctuation field $\tilde{u}_2$ that satisfies Equation (22), we can further constrain the fine-scale displacement field. In this paper, we choose the case where the kinematical constraint on the fine-scale mesh is $\tilde{u}_2 = 0$. Following Equation (20), we have

$$\boldsymbol{u}_2 = \boldsymbol{\varepsilon}_1 \boldsymbol{x}_2 \tag{23}$$

For displacement fields that satisfy Equation (23), it can be shown that the Hill's energy condition

$$\boldsymbol{\varepsilon}_1 : \boldsymbol{\sigma}_1 = \frac{1}{\text{meas}(\Omega)} \int_{\Omega} \boldsymbol{\varepsilon}_2 : \boldsymbol{\sigma}_2 \, d\Omega$$

is satisfied [23].

4.2. Element-splitting technique

In order to take into account material property fluctuations at higher resolution, the domain of interest at coarse scale needs to be further discretized. In the FEM, the domain of interest is discretized by coarse-scale elements. Naturally, the first step is to split coarse-scale FEs where needed. Consider a typical coarse-scale quadrilateral element as shown in the upper left corner of Figure 9. So-called 'ghost nodes' are first generated using the interpolation function as

$$\boldsymbol{x}^{\text{g}} = \boldsymbol{N} \cdot \boldsymbol{x}^{\text{FE node}} \tag{24}$$

where $\boldsymbol{x}^{\text{g}}$ is the position vector for ghost nodes, $\boldsymbol{N}$ is the interpolation function, and $\boldsymbol{x}^{\text{FE node}}$ is the FE nodal position vector.

The element is then subdivided into tributary areas based on the generated ghost points and the existing FE nodes, e.g. shadow area in the coarse-scale element in Figure 9. Each of these tributary areas defines a domain for the finer scale, which is then further discretized using a new FE mesh. Therefore, each Gauss point at the coarse scale can be linked to a fine-scale mesh through element splitting. The information passing between these two scales will be described in the next section.

At this point, material properties at different levels of resolution will be needed and hence the method described in Sections 2 and 3 is utilized. The levels of resolution at the FE and the random

field are set to match each other at each scale. Moreover, each material point in the random field is set to be at the centroid of an FE so that each element has constant material properties.

4.3. Concurrent information-passing scheme

Once the domain is discretized, a systematic way to access information at multiple scales is needed. Here, we propose using a concurrent information-passing scheme where essentially displacements from coarser scale are passed onto the finer scale as boundary conditions and the averaged stress is passed back from the finer scale up to the coarser scale.

The first step of this scheme is to precondition the fine-scale mesh by a homogeneous state of strain ε_1^n and internal variables ξ_1^n, which correspond to the converged state at previous time station t_n of the coarse-scale Gauss point, i.e.

$$\varepsilon_2^0 = \varepsilon_1^n; \quad \xi_2^0 = \xi_1^n \tag{25}$$

where the superscripts '0' refers to the initial substep at the fine-scale computation and 'n' refers to the nth time step at coarse-scale computation.

This precondition step is necessary for the fine-scale computation to start from the same state as the corresponding Gauss point at the coarse scale. Following Equation (23), displacements Δu are imposed on the fine-scale FE mesh by

$$\Delta u_2 = \Delta \varepsilon_1 \cdot x_2 \tag{26}$$

where Δu_2 is the applied displacement boundary condition on the fine scale, $\Delta \varepsilon_1$ is the strain increment of the coarse-scale Gauss point, and x_2 is the position vector of the fine-scale mesh. Equation (26) means that the fine-scale displacement field is constrained to follow the coarse-scale displacement field at the boundary. The imposed displacements define a new boundary value problem, where the domain is the tributary area of the coarse-scale element.

Then, the fine-scale stress $\sigma_2(x)$ is computed from the constitutive equation with the prescribed strain ε_2^0 and the boundary condition Δu_2. Upon the completion of the fine-scale FE computation, the coarse-scale stress is then obtained by the homogenization equation, i.e.

$$\sigma_1 = \frac{1}{\text{meas}(\Omega)} \int_\Omega \sigma_2(x) \, d\Omega \tag{27}$$

As we employ FEs at both scales, we rely on the Newton–Raphson iterative algorithm to solve nonlinear problems. A consistent tangent operator (CTO) is needed for nonlinear FE analyses. In general, the CTO is defined as

$$c := \frac{\partial \sigma}{\partial \varepsilon} \tag{28}$$

where σ and ε are stress and strain tensors, respectively.

When we invoke the multi-scale computation for a particular coarse-scale element, to compute the corresponding CTO for the coarse scale, we use Equations (27) and (28), and take into account the assumption that a homogeneous state of strain and strain increments are applied:

$$\begin{aligned} c_1 :&= \frac{\partial \sigma_1}{\partial \varepsilon_1} \\ &= \frac{1}{\text{meas}(\Omega)} \int_\Omega \frac{\partial \sigma_2}{\partial \varepsilon_2} : \frac{\partial \varepsilon_2}{\varepsilon_1} \, d\Omega \\ &= \frac{1}{\text{meas}(\Omega)} \int_\Omega c_2 : I \, d\Omega \\ &= \frac{1}{\text{meas}(\Omega)} \int_\Omega c_2 \, d\Omega \end{aligned} \tag{29}$$

where I is the fourth-order identity matrix.

Finally, the averaged stress and CTO are passed back to the Gauss point at the coarse scale for global stiffness and residual matrices assembly. Figure 9 summarizes the above-described multi-scale framework.

The above-described scheme will allow one to systematically refine the domain of interest and passing information from field scales all the way to specimen and mesoscales. The selective refining strategy, on the other hand, would allow for a more efficient solution where details are only resolved when necessary. The idea here is to zoom into zones where intense deformation is taking place. Identifying those 'key areas' is a nontrivial task and may require an error estimator and an adaptive algorithm, which is beyond the focus of this paper. Here, we will loosely define such key areas through the deterministic study. For the footing problem shown later, we know *a priori* to a good extent where the intense deformation occurs.

5. NUMERICAL SIMULATIONS

In this section, we present numerical simulations of a typical footing problem utilizing random fields and the FEM at multiple scales. The geometry of the problem is 20×8 m, which is discretized by a coarse-scale FE mesh. A rough rigid footing on cohesive weightless soil is modeled with width of the footing (B) being 4 m. A Drucker–Prager model [24] is used to describe the elasto-perfectly plastic behavior of the soil. The friction angle in the following simulations is set to be zero for simplicity. Soil properties needed in the mechanical model are Young's modulus E, Poisson's ratio v, and the undrained shear strength S_u. Both the bearing capacity and the settlement of the footing will be analyzed. S_u and E could be modeled as cross-correlated random fields for higher accuracy, e.g. via suitable correlation functions. However, it is known that S_u is the dominant factor in bearing capacity analysis, while E is the dominating factor in settlement analysis. To simplify the analysis and to focus on the effect of randomness across different scales, S_u is treated as the only spatially correlated random variable in the bearing capacity analysis with constants (deterministic) E and v, while E is treated as a correlated random field in settlement analysis with S_u and v being constant and deterministic.

The objective of this footing problem is to utilize the above-described framework to study the effect of random fields on the performance of the geosystem in a multi-scale context. In particular, the influence of considering finer scale random fields will be analyzed. In the following simulations, three length parameters are of particular interest to the analysis, i.e. a, L_1, and L_2, where a is the parameter related to spacial correlation (Equation (5)) and larger value of a indicates a more smoothly varying field; L_1 is the size of a coarse-scale element, which is a constant in this paper ($L_1 = 0.5$ m); and L_2 is the size of a fine-scale element, which depends on the degree of discretization. The degree of discretization (ds) indicates how quickly a coarse-scale cell will be refined. For example, $ds = 4$ means a 1×1 cell at the coarse scale will be refined to 4×4 smaller pieces at the fine scale.

5.1. Deterministic study

A deterministic study was first carried out using single-scale FEs (at the coarse scale) to obtain the deterministic bearing capacity and settlement, and to identify possible 'key areas' that will be linked to fine-scale information. Material properties used are Young's modulus $E = 100$ MPa, Poisson's ratio $v = 0.3$, and the undrained shear strength $S_u = 100$ kPa.

Typical load–displacement curves are shown in Figure 10. Here, failure is said to occur when further loading no longer increases the bearing pressure (within a very small tolerance). It can be seen from Figure 10 that as the mesh is refined, the bearing capacity will converge to the value calculated by Prandtl's solution, $q_f = N_c S_u = 514$ kPa. Taking into account both accuracy and efficiency, we choose a coarse-scale mesh of 40×16 elements, as shown in Figure 11, for all simulations in the following sections. The deterministic bearing capacity for this mesh is $q_d = 556.27$ kPa, which is about 8% higher than that given by Prandtl. For rigid rough footing condition simulated here, the footing nodes settle vertically by the same amount with no rotation.
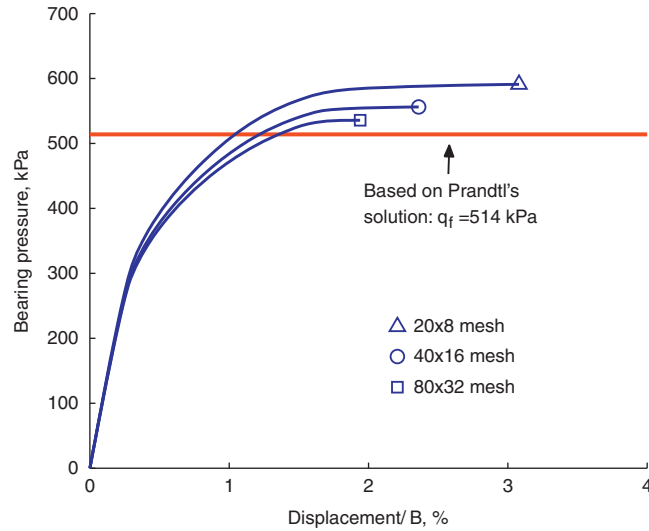
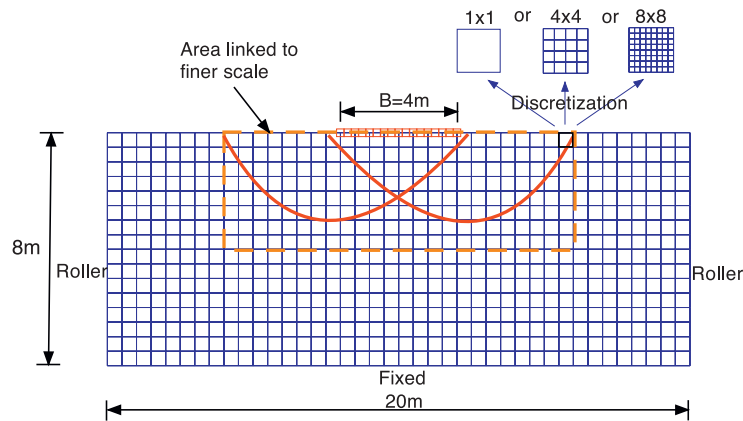Figure 10. Load–displacement curves for a strip footing on homogeneous soil.

Figure 11. The coarse-scale finite element mesh (40×16) and the area linked to the finer scale.

When loading pressure on the footing equals 300 kPa, the deterministic settlement δ_{det} equals to 0.012 m, which can be normalized by the width of the footing, i.e. $\delta_{det}/B = 0.003$. In simulations utilizing random fields, the settlement at 300 kPa loading pressure will be obtained and compared with this deterministic value.

Figure 12 shows the deviatoric strain contour at failure. Intense deformation occurs at the edge of the footing and failure surfaces are clearly formed. The 'key area' is therefore chosen to encompass the intense deformation zone and the failure surfaces, as shown in the dashed box in Figure 11. The geometry of this area is 12×4 m. Also shown in Figure 11 are different levels of discretization.

5.2. Influence of multi-scale random fields on bearing capacity

In this section, the multi-scale random fields and the FEM are incorporated to simulate the footing problem. An initial coarse-scale random field for the undrained shear strength is generated using 40×16 grids and hence matching the FE resolution. Three coarse-scale correlation length parameters (normalized), i.e. $a/L_1 = 0.5$, 1.0, and 2.0 will be considered when generating random fields. In the 'key area', the fine-scale resolution will be different depending on the degree of discretization. Three particular cases with $ds = 1$, 4, and 8 are considered. The coarse-scale FE mesh will be split accordingly as shown in Figure 11 to match the random field resolution.
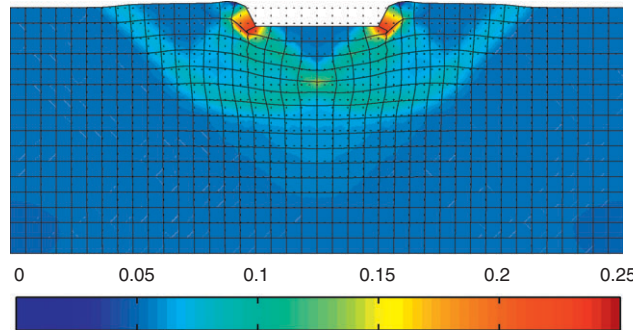
Figure 12. Deviatoric strain contour at failure for a deterministic study.

Material parameters for generating lognormally distributed random fields are the mean $\mu =$ 100 kPa, which equals to the shear strength value used in the deterministic study, and the standard deviation $\sigma = 50$ kPa, which gives the coefficient of variation (COV) a value of 0.5. Constant material properties are Young's modulus $E = 100$ MPa and Poisson's ratio $v = 0.3$.

The initial random field simulation will first generate a coarse-scale resolution for the entire domain. This field will be referred to as 'coarse-scale random field'. Within the 'key area', the framework described in Section 3 will be used to resolve the coarse-scale points down to finer pieces according to specified degree of discretization. The generated random field after this refinement process will be referred to as 'multi-scale random field'. Through comparison of these two types of random fields, we will show how considering finer scale information will influence the mechanical behavior of the whole system.

Typical realizations of initial undrained shear strength fields for different degrees of discretization are shown in Figure 13 for $a/L_1 = 2.0$. Coarse-scale random fields are on the left column and corresponding multi-scale random fields are on the right column. The degree of discretization increases from top to bottom.

Although the same material parameters, i.e. μ and σ, are used for generating every random field in this paper, they are defined at different length scales for different degrees of discretization. For every realization, we can compute the mean and standard deviation of each generated random field as well as the averages of those mean and standard deviation values, as shown in Figures 14 and 15. Moreover, those averaged values can be used in approximating mean bearing capacities [25].

The idea is to start from the simplified bearing capacity equation, where soil is assumed to be weightless, then

$$q_f = S_u N_c \tag{30}$$

If we assume Prandtl's solution for frictionless soil (as is the case in this paper) holds, then Nc is constant ($N_c = 5.14$). Take natural logarithm of Equation (30)

$$\ln q_f = \ln S_u + \ln N_c \tag{31}$$

The mean of $\ln q_f$ is therefore

$$\mu_{\ln q_f} = \mu_{\ln S_u} + \mu_{\ln N_c}$$

$$= \ln \mu_{S_u} - \frac{1}{2}\ln\left(1 + \frac{\sigma_{S_u}^2}{\mu_{S_u}^2}\right) + \ln N_c \tag{32}$$

Then the mean of q_f can be approximated as

$$\mu_{q_f} = \exp\{\ln N_c + \ln \mu_{S_u} - \tfrac{1}{2}\ln(1 + \sigma_{S_u}^2/\mu_{S_u}^2)\} \tag{33}$$

This approximated analytical mean value of bearing capacity will be plotted with the results obtained by FEM computation as will be shown later.
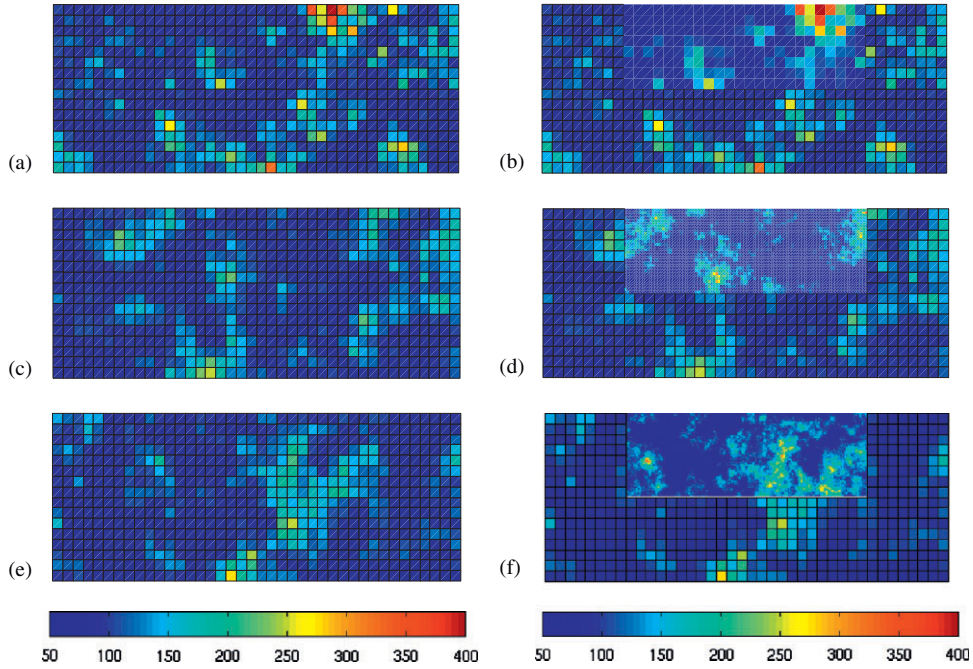
Figure 13. Initial undrained shear strength fields for $a/L_1 = 2.0$ with different degrees of discretization: from top to bottom: $ds = 1$, 4, and 8, respectively, with the left column being coarse-scale random fields and the right column being multi-scale random fields.
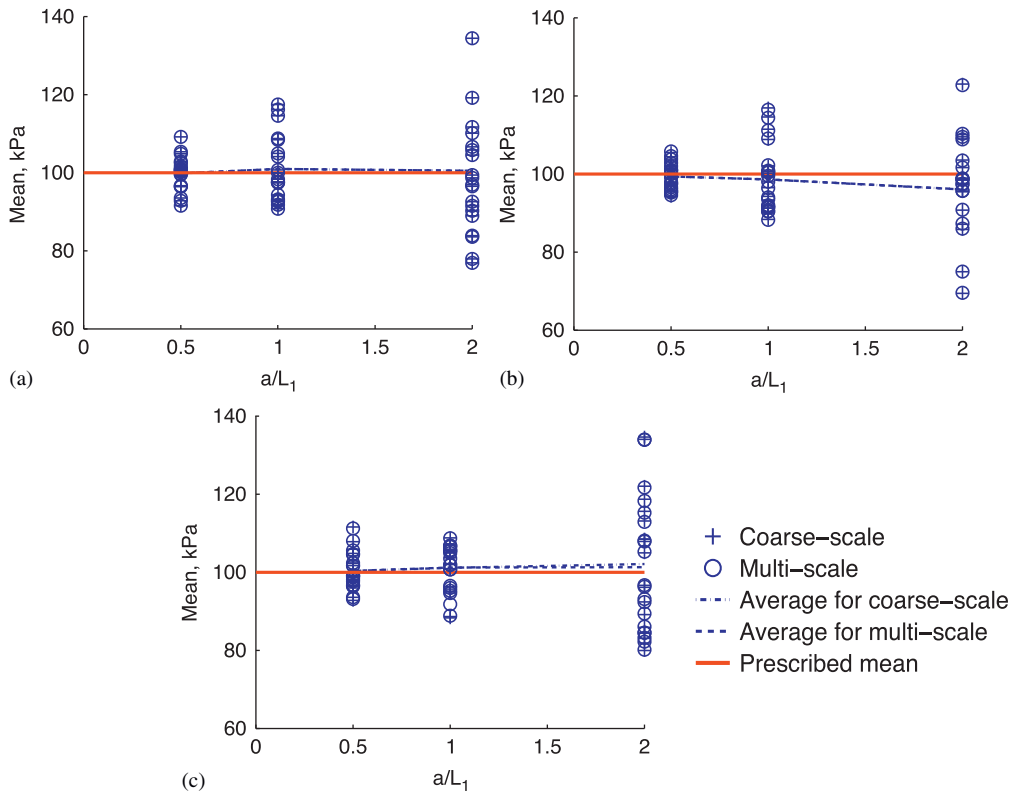

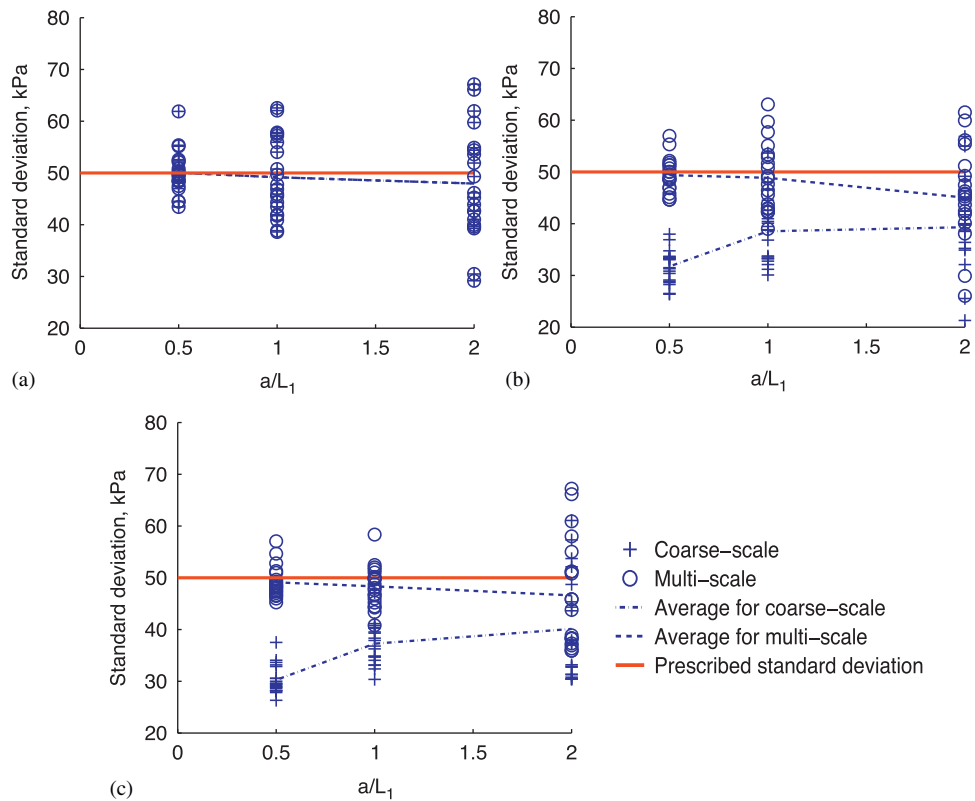Figure 14. Mean for the generated initial undrained shear strength: (a) $ds = 1$; (b) $ds = 4$; and (c) $ds = 8$.

Figure 15. Standard deviation for the generated initial undrained shear strength:
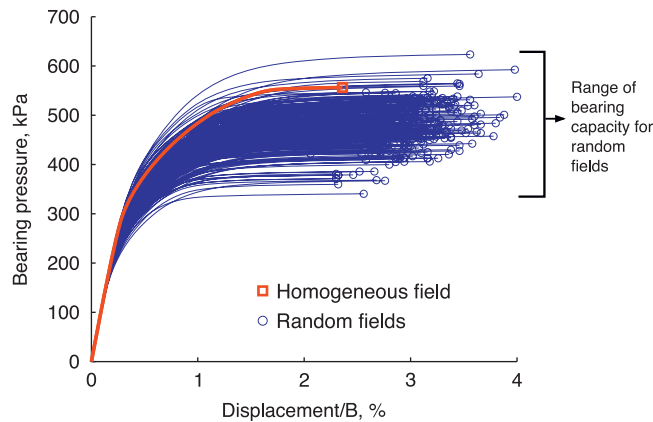(a) $ds = 1$; (b) $ds = 4$; and (c) $ds = 8$.

Figure 16. Load–displacement curves for all simulations.

The load–displacement behavior obtained by random fields and deterministic analyses is shown in Figure 16 for all simulations. It can be seen that bearing capacities of spatially varying soil are significantly lower (18% on average) than the corresponding deterministic value.

Figure 17 shows how bearing capacities change with a/L_1 for different degrees of discretization. The first observation is that the mean bearing capacities computed by Equation (33) are in good agreement with the FEM results especially for multi-scale cases, which shows Equation (33) can be used as a rough estimation of mean bearing capacities. Also, it can be seen that (1) for coarse-scale results with the same discretization level, the averaged bearing capacity increases
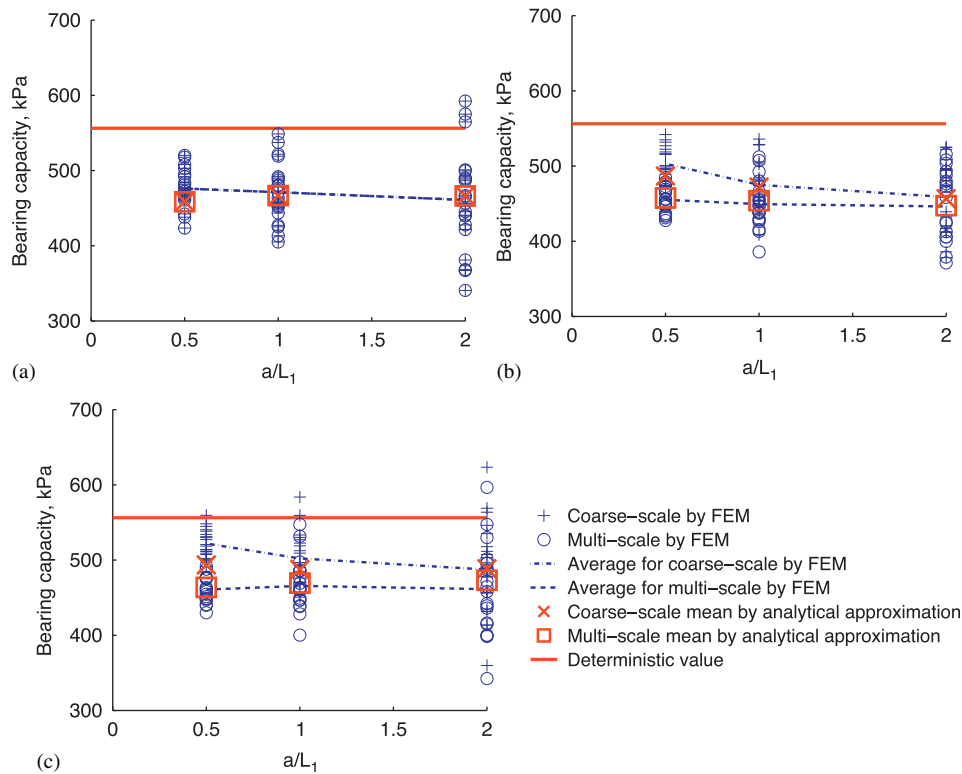
Figure 17. Bearing capacities for different degrees of discretization: (a) $ds=1$; (b) $ds=4$; and (c) $ds=8$.

slightly as a/L_1 decreases, this observation is consistent with the standard deviation curve shown in Figure 15, where smaller value of a/L_1 gives a lower standard deviation and, therefore, a stronger field and (2) for coarse-scale results with the same a/L_1, the averaged bearing capacity increases with ds. This is because the coarse-scale data point is seen as the average of the fine-scale points. The averaging process effectively reduces the variability, especially for larger values of ds, which is shown in Figure 15 where the standard deviations for $ds=4$ and 8 are smaller than that of $ds=1$ for the same a/L_1 values. While the mean values are roughly the same for all simulations, the reduced variability will result in stronger fields that lead to higher bearing capacities.

Even more important observation in Figure 17 is the effect of using multi-scale random fields. It can be seen that the mean of the bearing capacities obtained by multi-scale computation is not influenced as much by either ds or a/L_1. This is because the mean of the bearing capacities is mainly affected by the mean and standard deviation of the undrained shear strength fields, which as shown in Figures 14 and 15, is not significantly sensitive to either ds or a/L_1. Furthermore, with ds and a/L_1 being the same, multi-scale bearing capacity results are, in general, smaller than coarse-scale ones, especially for smaller values of a/L_1. The reason is that, instead of using a local average of the material properties, multi-scale computations zoom into the specific area to obtain more detailed fine-scale information, which has roughly the same mean but higher variability than their coarse-scale counterparts (as shown in Figures 14 and 15). Therefore, this results in weaker zones that lead to lower bearing capacities. Also, the trend that the difference between coarse-scale and multi-scale bearing capacities decreases as a/L_1 increases is consistent with the trend observed in the standard deviation of generated data shown in Figure 15. The above observations confirm that using averaged coarse-scale material properties tends to overestimate the bearing capacity. In other words, coarse-scale results are less conservative.

Figure 17 shows how the bearing capacities are influenced by multi-scale random fields with different levels of discretization. However, it does not provide information about how the failure
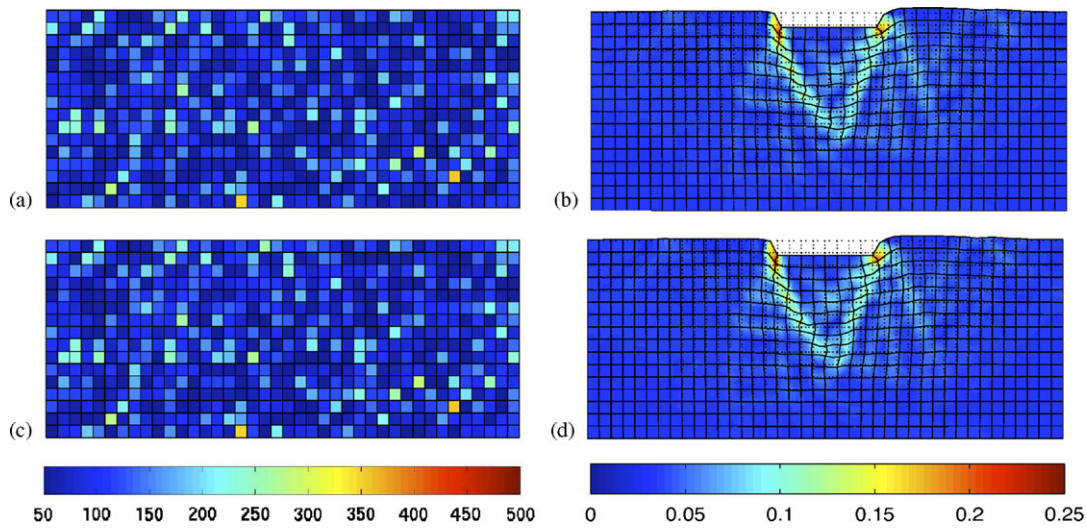
Figure 18. Comparison between coarse-scale and multi-scale random fields on failure surface for $a/L_1 = 0.5$ with $ds = 1$: left column are initial shear strength fields and right column are shear strain contours at failure. (a) and (b) correspond to coarse scale and (c) and (d) correspond to multi-scale.
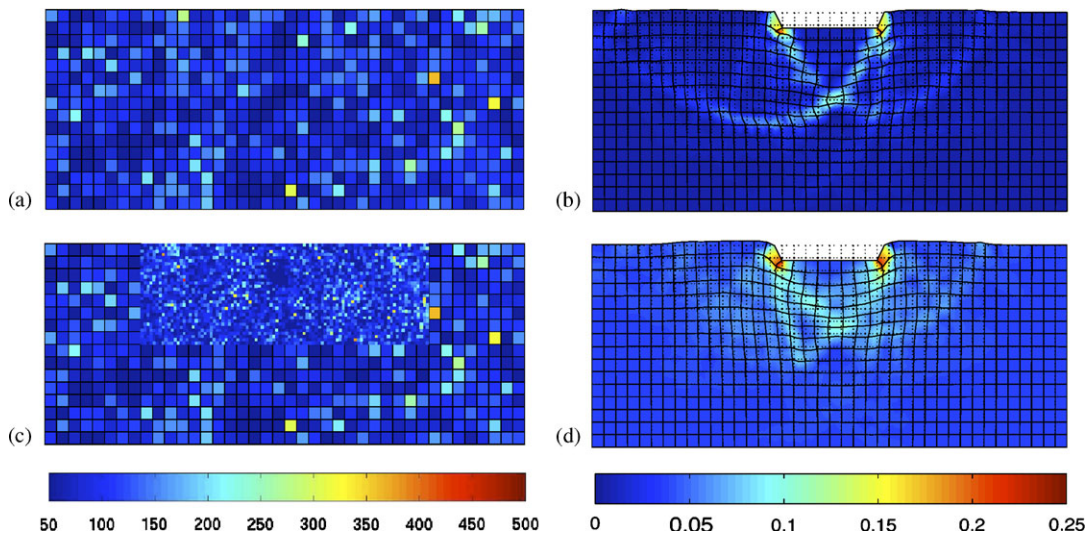

Figure 19. Comparison between coarse-scale and multi-scale random fields on failure surface for $a/L_1 = 0.5$ with $ds = 4$: left column are initial shear strength fields and right column are shear strain contours at failure. (a) and (b) correspond to coarse scale and (c) and (d) correspond to multi-scale.

surfaces are affected by considering the random field at multiple scales. Such insight is provided in Figures 18–20, which show the deviatoric strain contours for one particular realization for $a/L_1 = 0.5$ with $ds = 1$, 4, and 8. Unsymmetrical failure surfaces can be clearly seen in these figures. In the literature, e.g. [2–4], effects of single-scale random fields on formation of failure surfaces are studied. It has been shown that spatially varying soil properties trigger unsymmetrical failure surface passing mainly through weaker soil zones. Figures 18–20 show clearly these trends. More interestingly, these figures show that in multi-scale random cases there are more local fluctuations in the shear strains than in the coarse-scale cases, because higher levels of resolution are taken into account. This detailed information may lead to effectively weaker spots resulting in lower bearing capacities.
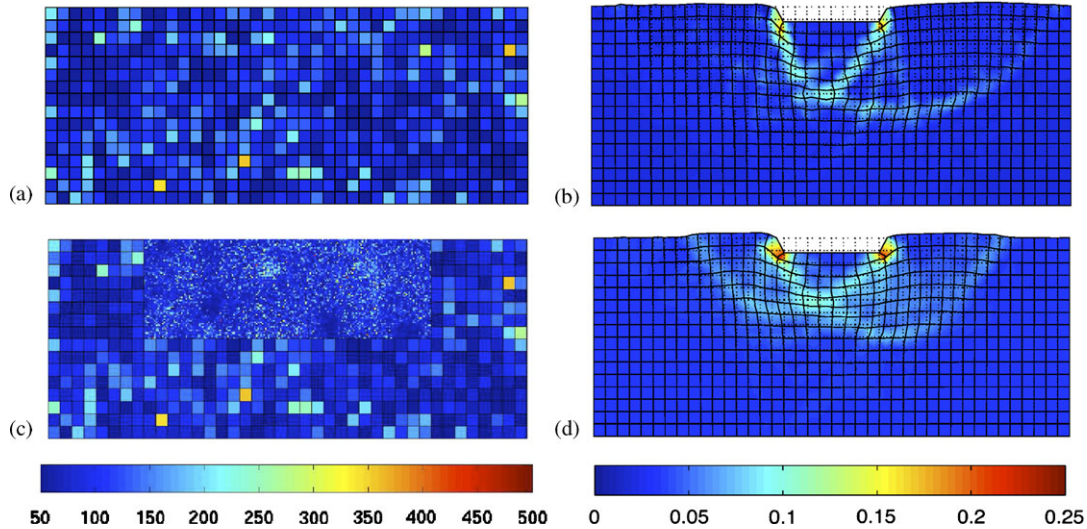
Figure 20. Comparison between coarse-scale and multi-scale random fields on failure surface for $a/L_1 = 0.5$ with $ds = 8$: left column are initial shear strength fields and right column are shear strain contours at failure. (a) and (b) correspond to coarse scale and (c) and (d) correspond to multi-scale.

5.3. Influence of multi-scale random fields on settlement

In this section, the influence of multi-scale random fields on settlement is analyzed. For this purpose, Young's modulus E is treated as the random variable while v and S_u are held constant. Material parameters for generating lognormally distributed Young's modulus fields are the mean $\mu = 100$ MPa, which is equal to the values used in the deterministic study, and standard deviation $\sigma = 50$ MPa, which gives a COV value of 0.5. Three correlation length parameters (normalized) $a/L_1 = 0.5$, 1.0, and 2.0 are used. The process for generating random fields, the definition of degree of discretization, and the notation for results are exactly the same as those used in bearing capacity analysis. We look at the variations in settlement at a pressure level of 300 kPa.

Typical realizations of initial Young's modulus fields for different degrees of discretization are shown in Figure 21 for $a/L_1 = 2.0$. Coarse-scale random fields are on the left column and corresponding multi-scale random fields are on the right column. The degree of discretization increases from top to bottom.

Figure 22 shows settlements versus a/L_1 for different degrees of discretization. The settlements are normalized by the width of the footing. Analogous to bearing capacity analysis, it can be seen that (1) for coarse-scale results with the same discretization level, the averaged settlement increases as a/L_1 increases; (2) for coarse-scale results with the same a/L_1, the averaged settlement decreases with increasing ds; (3) for $ds = 1$, there is no difference between coarse-scale and multi-scale results as expected; and (4) for $ds = 4$ and 8 cases, higher levels of resolution are taken into account in multi-scale computations and the results show that the multi-scale random fields yield larger settlements on average for every value of a/L^1, which confirms that coarse-scale results are less conservative.

Remark 1

Sections 5.2 and 5.3 explore the effects of changing resolution for the specific examples presented in this paper. Generally, increasing number of fine-scale elements within a coarse-scale element will result in lower bearing capacity (in bearing capacity analysis) and higher settlement (in settlement analysis). In this formulation, the correlation length sets the macroscopic size of the elements. In essence, the element size should be such as to be able to resolve the gradients in the stochastic field. This is accounted for in our analysis. As for the effect of the RVE size, this formulation does not determine or sets the size of RVE, this is something that would rather be problem dependent
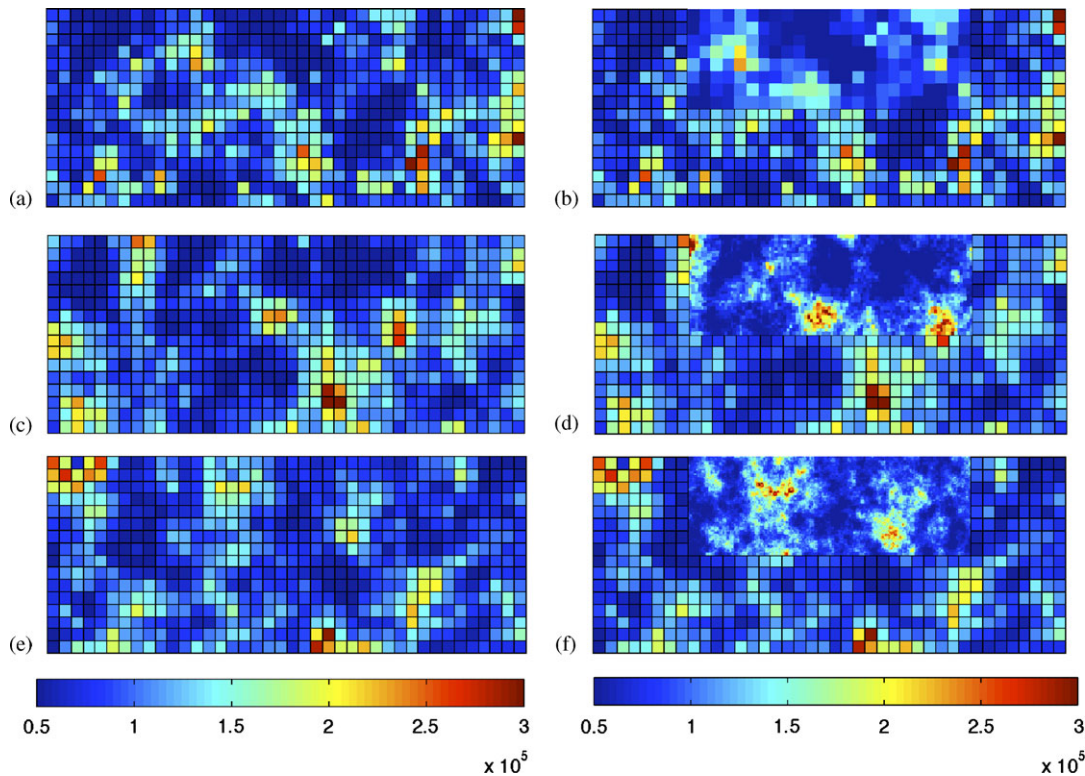
Figure 21. Initial Young's modulus fields for $a/L_1 = 2.0$ with different degrees of discretization: from top to bottom: $ds = 1$, 4, and 8, respectively, with left column being coarse-scale random fields and right column being multi-scale random fields.

and determined by the correlation lengths and the deformation gradient in the problem. Interested readers may refer to [26] for discussions on selecting the size of the averaging window.

6. CONCLUSIONS

In this paper, we presented a novel method for characterizing multi-scale random fields. CDFs and spatial correlation for two soil properties of interest, undrained shear strength and Young's modulus, were described at the finest considered scale. The relationship between this scale and a coarser scale was defined and incorporated into a sequential simulation procedure. While two scales were presented here, including more by expanding the multi-scale definitions is straightforward, and there is no need to specify the number of scales in advance. Simulations begin at the coarse scale and work towards higher resolution, but the results are indiscernable from starting at the fine scale and averaging those elements together. For convenience, a correlated standard Gaussian field was initially generated and then transformed to the target distribution via normal-score mapping.

We then proposed a framework for coupling the FEM with random fields at multiple scales. The formulation of the framework is based on the assumption that the strain and the stress at an arbitrary material point in the coarse-scale domain are the volume average of the strain and stress fields over the fine-scale domain, respectively. The framework consists of an element-splitting technique and a concurrent information-passing scheme. A selective refining strategy was used so that resolution is only increased where necessary.

A total of 720 simulations were performed. Among them, half utilized the proposed multi-scale framework and the other half utilized coarse-scale random fields for comparison purposes. Bearing capacity and settlement analyses were performed using the undrained shear strength and
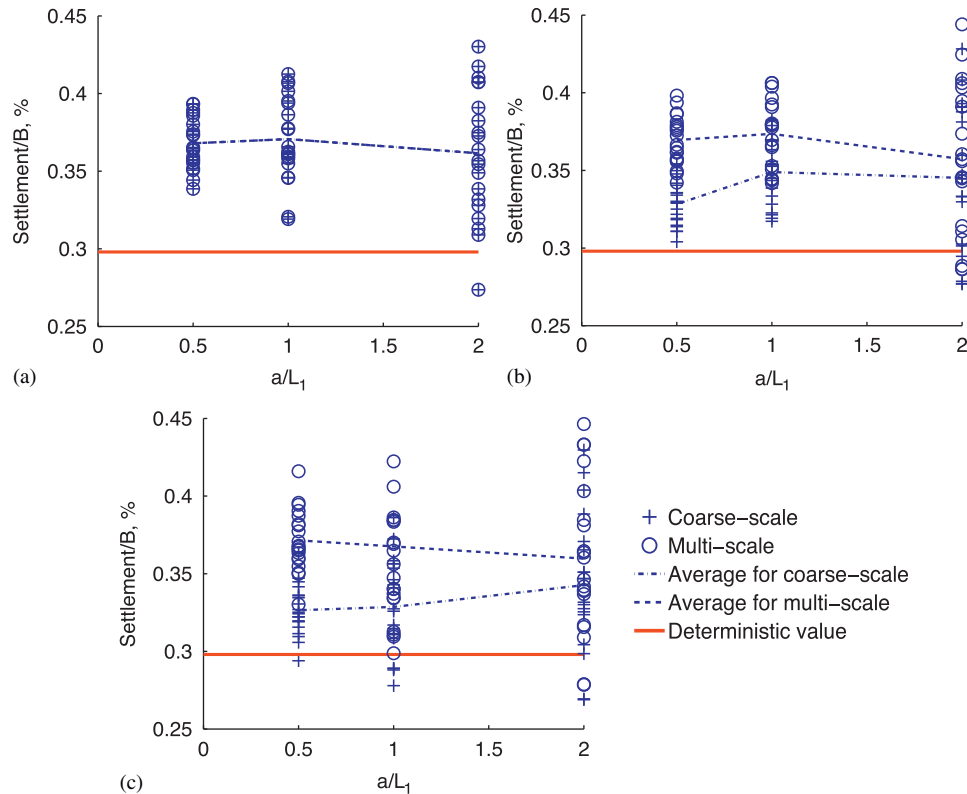
Figure 22. Settlements for different degrees of discretization: (a) $ds=1$; (b) $ds=4$; and (c) $ds=8$.

the Young's modulus as the random variable, respectively. It was shown that material property fluctuations, in general, will result in lower bearing capacities, unsymmetrical failure surfaces, and larger settlements. More importantly, multi-scale results show that higher levels of resolution result in lower bearing capacities and larger settlements. Or in other words, coarse-scale results are generally less conservative. These results show how the mechanics of the geosystem is influenced by multi-scale random fields and the importance of accounting for material inhomogeneities at different scales.

REFERENCES

1. Andrade JE, Baker JW, Ellison KC. Random porosity fields and their influence on the stability of granular media. *International Journal for Numerical and Analytical Methods in Geomechanics* 2008; **32**:1147–1172.
2. Griffiths DV, Fenton GA. Bearing capacity of spatially random soil: the undrained clay Prandtl problem revisited. *Géotechnique* 2001; **51**(4):351–359.
3. Griffiths DV, Fenton GA, Manoharan N. Bearing capacity of rough rigid strip footing on cohesive soil: probabilistic study. *Journal of Geotechnical and Geoenvironmental Engineering* 2002; **128**(9):743–755.
4. Popescu R, Deodatis G, Nobahar A. Effects of random heterogeneity of soil properties on bearing capacity. *Probabilistic Engineering Mechanics* 2005; **20**:324–341.
5. Shen L, Xu XF. Multiscale stochastic finite element modeling of random elastic heterogeneous materials. *Computational Mechanics* 2010; **45**:607–621.

6. Chen X, Xu XF, Shen L. A green-function-based multiscale method for uncertainty quantification of finite body random heterogeneous materials. *Computers and Structures* 2009; **87**:1416–1426.

7. Xu XF. A multiscale stochastic finite element method on elliptic problems involving uncertainties. *Computer Methods in Applied Mechanics and Engineering* 2007; **196**:2723–2736.

8. Mei X. Multiscale methods: bridging the scales in science and engineering. *Concurrent Coupling of Atomistic and Continuum Models*. Oxford University Press, 2009.

9. Feyel F, Chaboche JL. FE^2 multiscale approach for modelling of the elastoviscoplastic behaviour of long fibre SiC/Ti composite materials. *Computer Methods in Applied Mechanics and Engineering* 2000; **183**:309–330.

10. Feyel F. A multilevel finite element method (fe2) to describe the response of highly non-linear structures using generalized continua. *Computer Methods in Applied Mechanics and Engineering* 2003; **192**:3233–3244.

11. Ibrahimbegović A, Marković D. Strong coupling methods in multi-phase and multi-scale modeling of inelastic behavior of heterogeneous structures. *Computer Methods in Applied Mechanics and Engineering* 2003; **192**:3089–3107.

12. Marković D, Ibrahimbegović A. On micro-macro interface conditions for micro scale based FEM for inelastic behavior of heterogeneous materials. *Computer Methods in Applied Mechanics and Engineering* 2004; **193**:5503–5523.

13. Marković D, Niekamp R, Ibrahimbegović A, Matthies HG, Taylor RL. Multi-scale modeling of heterogeneous structures with inelastic constitutive behaviour. Part I: Physical and mathematical aspects. *Engineering Computations* 2005; **22**:664–683.

14. Andrade JE, Tu XX. Multiscale framework for behavior prediction in granular media. *Mechanics of Materials* 2009; **41**(6):652–669.

15. Andrade JE, Tu XX, Chen QS. Return mapping for nonsmooth and multiscale elastoplasticity. *Computer Methods in Applied Mechanics and Engineering* 2009; **198**:2286–2296.

16. Ladevèze P, Loiseau O, Dureisseix D. A micro-macro and parallel computational strategy for highly heterogeneous structures. *International Journal for Numerical Methods in Engineering* 2001; **52**:121–138.

17. Nemat-Nasser S, Hori M. *Micromechanics*: *Overall Properties of Heterogeneous Materials*. Elsevier: Amsterdam, the Netherlands, 1999.

18. Gitman IM, Askes H, Sluys LJ. Coupled-volume multi-scale modelling of quasi-brittle material. *European Journal of Mechanics A/Solids* 2008; **27**:302–327.

19. Goovaerts P. *Geostatistics for Natural Resources Evaluation*. Oxford University Press: New York, 1997.

20. Liu P, Der Kiureghian A. Multivariate distribution models with prescribed marginals and covariances. *Probabilistic Engineering Mechanics* 1986; **1**(2):105–112.

21. Vanmarcke E. *Random Fields*: *Analysis and Synthesis*. MIT Press: Cambridge, MA, 1983.

22. de Souza Neto EA, Feijóo RA. Variational foundations of multi-scale constitutive models of solids: small and large strain kinematical formulation. *Technical Report*, National Laboratory for Scientific Computing (LNCC), Brazil, 2006.

23. Zohdi TI, Wriggers P. An introduction to computational micromechanics. *Fundamental Micro-macro Concepts*. Springer: Berlin, 2005.

24. Drucker DC, Prager W. Soil mechanics and plastic analysis or limit design. *Quarterly of Applied Mathematics* 1952; **10**:157–165.

25. Fenton GA, Griffiths DV. The random finite element method (RFEM) in bearing capacity analysis. *Probabilistic Methods in Geotechnical Engineering*. Springer: Wien, New York, 2007.

26. Baxter SC, Graham LL. Characterization of random composites using moving-window technique. *Journal of Engineering Mechanics* 2000; **126**:389–397.